Impedance Analysis of the Hall Thruster Discharge Circuit and Plasma Load to Address Harness Facility Effects

IEPC-2024-619

Presented at the 38th International Electric Propulsion Conference
Pierre Baudis Convention Center • Toulouse, France
June 23-28, 2024

Ajay Krishnan[1], Dan R. Lev[2], and Maryam Saeedifard[3]
Georgia Institute of Technology, Atlanta, GA, 30332

Lukas Graber[4]
Georgia Institute of Technology, Atlanta, GA, 30332

and

Mitchell L. R. Walker[5]
Georgia Institute of Technology, Atlanta, GA, 30332

The wire harness is an important part of the discharge circuit, though its length can vary between ground and space, resulting in differences in discharge voltage oscillations and in the impedance of a Hall thruster discharge plasma. Though the conventional approach is to minimize the length of the harness by moving the location of the filter as close as possible to the thruster, this, however, is not always possible. We investigate the effects of harness inductance on discharge voltage and current oscillations in a Hall thruster using a 0D breathing mode model, which show that voltage oscillations continue to grow linearly to 40 $V_{pk\text{-}pk}$ at a harness inductance of 50 µH, while the current oscillations remain unchanged. Discharge voltage oscillations are shown to attain negative values at a harness inductance of 700 µH and a harness capacitance of 3.782 nF, respectively. We then use simulations driven by experimental discharge current data obtained from a H9 Hall thruster operated at a 6-kW condition of 300 V and 20 A at a harness inductance of 25.6 µH. We apply a linear time-invariant fast Fourier transform approach to compute impedance by dividing voltage and current in the frequency domain, which gives a transmission line characteristic with discharge resistance, inductance, and capacitance of 1.847 Ω, 52.336 µH, and 1.742 nF, respectively. The DC, breathing mode, and peak impedances are 14.25, 4.25, and 5.6 Ω, respectively. We also use the fast Fourier transform approach to determine reactive power at all frequencies, with the breathing mode oscillation at 14 kHz producing the most reactive power at 1.591 VAR. We generalize the frequency domain approach by applying the short-time Fourier transform to account for linear time-varying behavior and by utilizing the IMFogram method to analyze nonlinear time-varying behavior. Lastly, we outline the possibility of placing additional RLC networks in the discharge circuit to enable reactive compensation and impedance matching for maximum power transfer. This work serves to inform engineers about optimal harness design and more broadly optimal discharge circuit analysis and design strategies through an improved understanding of the discharge plasma load.

[1] Graduate Research Assistant, School of Electrical and Computer Engineering, ajaykrishnan@gatech.edu
[2] Research Engineer, School of Aerospace Engineering, dan.lev@gatech.edu
[3] Professor, School of Electrical and Computer Engineering, maryam@ece.gatech.edu
[4] Associate Professor, School of Electrical and Computer Engineering, lukas.graber@ece.gatech.edu
[5] Chair and Professor, School of Aerospace Engineering, mitchell.walker@ae.gatech.edu

Nomenclature

w = radian frequency
f = frequency
V = voltage
X = reactance
Z = impedance
ϵ_{ion} = ionization energy loss
ϵ_w = electron energy loss to the wall
ζ_{ion} = ionization rate coefficient
ν_w = electron wall collision frequency
χ = ionization cost
σ = rate of secondary electron emission
ϕ_w = sheath potential
T_e = electron temperature
U_e = electron bulk velocity
U_i = ion bulk velocity
$U_{i,w}$ = ion acoustic speed
U_n = neutral bulk velocity
R_Δ = channel width
M_i = ion mass
$\dot{m}$ = neutral mass flow rate
m_e = electron mass
N_i = ion number density
N_{int} = injected neutral number density at anode
N_n = neutral number density
L_{ch} = channel length
A_c = thruster cross-sectional area
E = electric field strength
e = fundamental charge
VP = Power Supply Voltage
CP = Power Supply Capacitance
RHP = Power Supply Harness Resistance
LHP = Power Supply Harness Inductance
CHP = Power Supply Harness Capacitance
RF = Filter Resistance
CF = Filter Capacitance
RHT = Thruster Harness Resistance
LHT = Thruster Harness Inductance
CHT = Thruster Harness Capacitance
ID = Discharge Current
V_d = Discharge Voltage
V_{Cf} = Filter Capacitor Voltage
I_{Lf} = Filter Inductor Current
I_{LH} = Harness Inductor Current
RDP = Discharge Plasma Resistance
LDP = Discharge Plasma Inductance
CDP = Discharge Plasma Capacitance

Subscripts

in = input

I. Introduction

A Hall effect thruster (HET) is an electrostatic plasma device that produces thrust via the acceleration of ions [1]. They were first developed in the 1960s and have since been increasingly adopted as a propulsion option for satellites due to their mass savings as compared to chemical propulsion systems [1]. To improve their use in satellites and deep space missions, it is necessary to advance HET technology by increasing thrust, specific impulse, efficiency, and thruster lifetime. The development of such propulsion technology requires operating HETs in dedicated vacuum facilities on the ground, and replicate conditions as close as possible to those expected in space. However, it is not possible to fully emulate space conditions on the ground, leading to unintended deviation from the performance and physics as measured in space [2].

The use of vacuum chambers introduces what is referred to as “facility effects” that change thruster performance and thruster plume and discharge physics on the ground compared to that in space [2]. Facility effects occur because ground facility pumping systems cannot reach the low-pressure levels as in space [3]. In addition, the existence of a large metal facility creates current paths that otherwise do not exist in the space environment [4, 5, 6]. Lastly, sputtering, coming from the chamber walls back onto and into the thruster may interfere with the discharge and affect HET lifetime [2]. Thus, it is necessary to understand the influence of different facility-related factors on HET physics and operation and to be able to correct performance on the ground to determine performance in space. In this study, we specifically focus on harness facility effects, which result from different wire harness lengths and, thus, different harness inductances between ground and space operation of HETs.

Discharge current oscillations are the result of plasma instabilities in the discharge of a HET [7]. Of the various types of HET oscillations, the predominant type is the so-called “breathing mode” oscillations that are tied to predator-prey interactions between neutrons and electrons in the plasma. They present variations in plasma parameters, specifically plasma density, in the discharge chamber of the thruster. The dynamics of the breathing mode oscillations (BMO) can be expressed by the conservation of mass, momentum, and energy equations and used to define the discharge plasma as an electrical load [8]. This dominant mode occurs in the tens of kHz range and can lead to discharge current amplitudes of over 100% of the mean [9]. It plays a significant role in the dynamics

The 38th International Electric Propulsion Conference, P. Baudis Convention Center, Toulouse, France June 23-28, 2024

and performance of a Hall thruster, as highly oscillatory thrusters show degraded performance.

Discharge voltage oscillations are the result of discharge current oscillations flowing through harness inductance. The relation can be seen in Equation 1.

$$V = L\frac{\mathrm{dI}}{dt} \tag{1}$$

They could potentially be hazardous to the thruster if they exceed its voltage rating.

Past work on harness analysis was performed by Luis Pinero at the NASA Glenn Research Center and by Dr. Lubos Brieda [10, 11]. Pinero focused on an experimental approach while Brieda focused on a simulation approach. Pinero used a breakout box with changeable components to vary the inductance of the harness. Pinero and Breida determined that voltage oscillations scale linearly with inductance at lower inductances, but as inductance increases, Brieda shows that voltage oscillations begin to decrease. This might be due to nonlinear effects between the harness inductance and the discharge plasma, where current oscillations are reduced, leading to reduced voltage oscillations. However, Brieda's computational results have not been verified experimentally.

Past work on impedance analysis was done by Jovel and Cabrera, where the primary assumption was that the Hall thruster under analysis was small-signal linear at specific operating points [12]. Rather than using a specialized hardware setup, our work uses frequency domain calculations from time series data alone. Fast Fourier transform (FFT) methods have been used in past work by those in the field of electrochemistry to compute the impedance of batteries. This process is called electrochemical impedance spectroscopy, where various AC injections are applied simultaneously to compute impedance through the division of voltage and current FFTs [13]. The short-time Fourier transform has also been used to perform such calculations, which also consider time varying effects. Nonlinear time-frequency analysis methods such as the empirical mode decomposition (EMD) and the Hilbert-Huang transform (HHT) have been used in the past to analyze Hall thruster data, but they were not applied to discharge voltage and current oscillations [14]. The IMFogram, developed by Cicone and Zhou at the Georgia Institute of Technology, offer an improvement for EMD and HHT [15].

This paper presents a computational and experimental effort using a 0-D BMO model and thruster discharge current measurements to determine the influence of discharge circuit impedance on the discharge voltage, discharge current, and discharge plasma impedance of a H9 HET (9 kW). We outline how RLC networks can be placed in between the discharge filter and the load as a form of passive control for the Hall thruster system by minimizing reactive power, rather than just solely placing the discharge filter close to the thruster. The total impedance of the circuit, which includes the filter and the harness, affects the dynamics of the load. We also show that FFT and STFT approaches can be used to effectively compute the impedance of a Hall thruster discharge plasma under different assumptions. Lastly, we demonstrate how the IMFogram technique can be used to represent a nonlinear time-varying system in the time-instantaneous frequency domain.

II. BMO Harness Model MATLAB Simulations

Section A discusses the transmission line analysis that can be applied to electrical harnesses used in the discharge circuit. Section B outlines the simulation setup, specifically the discharge circuit, used to conduct the BMO analysis. Section C delves into the 0D ionization model used for determining the effects of harness inductance on discharge voltage and current oscillations along with impedance. Section D discusses the FFT impedance characterization approach that can be used to characterize HET discharge plasmas along with its advantage over sinusoidal injection-based approaches. Lastly, section E discusses the concept of reactive power in a load with many frequency components and how reactive power compensation can lead to improvements in Hall thruster operation.

A. Transmission Line Analysis

Transmission lines are defined by a forward path and a return path to transmit power from source to destination. They can be made of copper wire or even other materials such as silver. AWG 6 electrical harness typically has a resistance, inductance, and capacitance per unit meter of roughly 3 mΩ/m, 0.4 µH/m and 59 pF/m, respectively [10].

The circuit analysis performed on a transmission line depends on its wavelength. If the length of the transmission line is less than the wavelength, then the circuit model is lumped. If it is greater, then the model is distributed. In the VTF-2 setup, the harness is approximately 64 m in length. The circuit model can be taken to be lumped for frequencies up to 4.5 MHz and is shown in figure 2 in the subsequent section. It is important to note that this model is a simplification and was used for simplicity. Flat lines in log-log plots of impedance versus frequency represent resistance, while lines with positive slope represent inductance, and lastly lines with negative slope represent

capacitance. A resonant peak is formed when inductive and capacitive behaviors meet, as shown in figure 1 for the harness used in the VTF-2 setup.

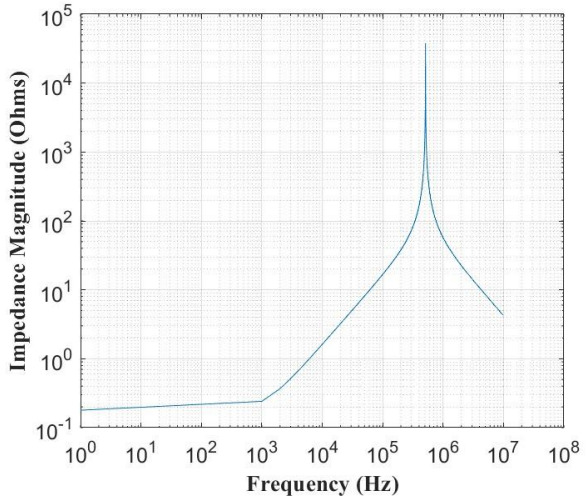

Figure 1 – Impedance-Frequency Plot for VTF2 Harness

B. Simulation Setup

Figure 2 shows the discharge circuit that was used to simulate the BMO model in MATLAB. All simulation settings match the 200 V case presented in Troyetsky et al., though we add harness RLC effects to it along with using a RC filter rather than a RLC filter [16]. RHT is given by 179 mΩ, LHT by 25.641 µH, CHT by 3782 pF, RF by 0.533 Ω, CF by 100 µH, and CP by 300 µH. The power supply harness may be neglected as it presents an insignificant effect given proper filter design that leads to almost DC conditions upstream from it. We note that the RLC transmission line that we use is a simplification; more effects can be considered but would further complicate the model.

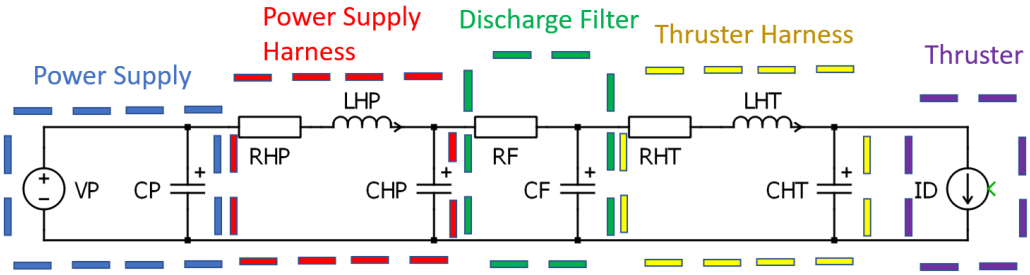

Figure 2 – Discharge Circuit

C. 0-D Ionization Model

The 0-D ionization model, also known as the BMO, refers to a system of nonlinear ODEs that model the predator-prey breathing mode oscillation process using conservation of mass, momentum, and energy equations [16]. The equations below govern state variables such as ion number density, neutral number density, electron temperature, ion velocity, electron velocity, and electrical parameters such as filter capacitor voltage and inductor current, and harness inductor current and discharge voltage. Equations 7, 9, and 10 are where the harness model was incorporated into the nonlinear ODE system. Additionally, circuit equations were rewritten so that inductor current and capacitor voltage were the electrical state variables. It is evident that the electrical state variables have a direct effect on the solution to the nonlinear system of ODEs. Most importantly, they influence the plasma parameters of the Hall thruster discharge plasma. It is also important to note that this model is for the breathing mode alone, while there are many other frequencies present in the system.

Nonlinear and time-varying nature can be observed mathematically from the ODE system describing the state variables, since the system contains equations where one or more state variables are multiplied together, leading to nonlinearity, while the coefficients of the state variables in their respective differential equations do not have constant coefficients, leading to time variance. The system is marginally stable since the solution to the system is almost sinusoidal. The state equations are:

$$\frac{\partial N_i}{\partial \mathrm{t}} = -\frac{N_i U_i}{L_{ch}} - \frac{2N_i U_{i,w}}{R_\Delta} + N_i N_n \zeta_{ion} \tag{2}$$

$$\frac{\partial N_n}{\partial \mathrm{t}} = -\frac{(N_n - N_{int})U_n}{L_{ch}} - N_i N_n \zeta_{ion} \tag{3}$$

$$\frac{\partial T_e}{\partial \mathrm{t}} = \frac{2}{3N_i}\left[-N_i U_e \mathrm{E} - N_i \epsilon_w \nu_w - N_i N_n \zeta_{ion} \chi \epsilon_{ion} - \frac{3}{2} T_e \frac{\partial N_i}{\partial \mathrm{t}} - \frac{5}{2}\frac{N_i U_e T_e}{L_{ch}}\right] \tag{4}$$

$$\frac{\partial U_i}{\partial \mathrm{t}} = \frac{\mathrm{eE}}{M_i} + \frac{2U_{i,w}U_i}{R_\Delta} + N_n \zeta_{ion}(U_n - U_i) \tag{5}$$

$$\frac{\partial U_e}{\partial \mathrm{t}} = 0 \tag{6}$$

$$\frac{\partial V_{Cf}}{\partial \mathrm{t}} = \frac{I_{Lf}}{C_f} - \frac{I_{LH}}{C_f} + \frac{V_p - V_{Cf}}{R_f C_f} \tag{7}$$

$$\frac{\partial I_{Lf}}{\partial \mathrm{t}} = \frac{V_p - V_{Cf}}{L_f} \tag{8}$$

$$\frac{\partial I_{LH}}{\partial \mathrm{t}} = \frac{V_{Cf} - R_H I_{LH} - V_d}{L_H} \tag{9}$$

$$\frac{\partial V_d}{\partial \mathrm{t}} = \frac{I_{LH}}{C_H} - \frac{\mathrm{eA}_C N_i (U_i - U_e)}{C_H} \tag{10}$$

where

$$U_{i,w} = \sqrt{\frac{eT_e}{M_i}} \tag{11}$$

$$N_{int} = \dot{m}(M_i A_c U_n)^{-1} \tag{12}$$

$$\zeta_{ion} = \sqrt{\frac{8eT_e}{\pi m_e}}\left[AT_e^2 + Bexp(-\frac{C}{T_e})\right] \tag{13}$$

$$\epsilon_w = 2T_e + (1\text{-}\sigma)\phi_w \tag{14}$$

$$\nu_w = \frac{1}{R_\Delta}\sqrt{\frac{eT_e}{M_i}}\frac{1}{1-\sigma} \tag{15}$$

$$\sigma = \min\left(\frac{T_e}{25}, 0986\right) \tag{16}$$

$$\phi_w = T_e \ln\frac{1-\sigma}{\sqrt{2\pi m_e/M_i}} \tag{17}$$

$$I_d = \mathrm{eA}_C N_i (U_i - U_e) \tag{18}$$

D. Impedance Analysis of a Hall Thruster Load

Impedance is a frequency dependent parameter and only exists in the frequency domain. One cannot divide AC voltage and current in the time domain. Instead, the division can only be done in the frequency domain for linear time-

The 38th International Electric Propulsion Conference, P. Baudis Convention Center, Toulouse, France June 23-28, 2024

invariant (LTI) systems. Thus, it is possible to divide the FFT of the voltage by the FFT of the current to get the impedance, as shown in equation 19. R, L, and C can be extracted from the impedance plot by either setting a known equivalent circuit model impedance expression equal to experimental measurements and solving, or by taking points from each region of the impedance plot and calculating R, L, and C based on their impedance formulas in appropriate and corresponding regions.

$$Z(w) = \frac{\mathrm{V(w)}}{I(w)} \tag{19}$$

To compute the impedance of a HET load, it is necessary to find an operating point where the discharge plasma can be small-signal linearized. Furthermore, this is necessary since it is difficult to assume linearity at small time scales since FFT resolution would be greatly reduced. The AC components of the HET load are significantly smaller than the DC operating point, so the HET load is small-signal linear. This means that the HET load is a linear time-varying system. When the harness inductance increases, the oscillations increase in magnitude, making small-signal linearity invalid and result in the load being non-linear time-varying.

A past study investigated impedance characterization by injecting a known sinusoidal voltage into the discharge and measuring the resulting current response, thereby giving impedance [12]. A drawback of the approach is that the injection is performed using an isolation transformer, which changes the discharge circuit and the operating point of the thruster due to additional inductance on its secondary. An isolation transformer on the thruster side of the filter is not necessary since perturbations can be applied on the power supply side of the filter using a function generator-power amplifier setup or a programmable power supply. This would be used to check that the unperturbed discharge plasma itself is small-signal linear by successively applying perturbations and observing that the impedance does not change. Using an FFT approach eliminates the need for always having to use specialized impedance measurement equipment and provides a faster and non-invasive method for computing the impedance of a Hall thruster discharge plasma. It also provides higher frequency resolution. Additionally, it allows for time-varying analysis as well, which isn't possible with the prior approach.

The fast Fourier transform (FFT), the short-time Fourier transform (STFT), and the IMFogram are all methods that can be used to characterize signals in the frequency domain. However, each is applicable under only certain assumptions. Table 1 shows the types of systems each transform can be used on.

Table 1 – Transforms and their System Applicability

Transform	System
FFT	Linear, time invariant
STFT	Linear, time varying
IMFogram	Nonlinear, time varying

Improvements over the FFT exist with the STFT. These transforms capture the time varying nature of the Hall thruster plasma and plot magnitude as a function of not just frequency as seen with the FFT but also with time. An FFT represents an average frequency representation of a signal, but if the window size of the FFT were to be made smaller, with successive overlapping windows, one arrives at the STFT, which generates a time-frequency representation. One can reasonably use the FFT information in a STFT by taking a slice at one particular point in time. In signal processing, there exists a manifestation of the Heisenberg uncertainty principle as seen in physics, where one cannot have certainty in both time and frequency simultaneously. Time-frequency plots show how frequencies change with time and amplitude. Though the STFT and FFT provide reasonable results, other basis functions lend themselves to better usage in time-frequency analysis. One such option is the continuous wavelet transform (CWT), which uses a wavelet as its basis, whose central frequency is equivalent to a sinusoidal frequency [17, 18, 19].

The IMFogram uses the fast iterative filtering (FIF) algorithm to generate intrinsic mode functions (IMFs) as an adaptive basis, with a subset of just three IMFs shown in figure 3, which can then be fed into the IMFogram algorithm to plot them in the time-frequency plane [15].

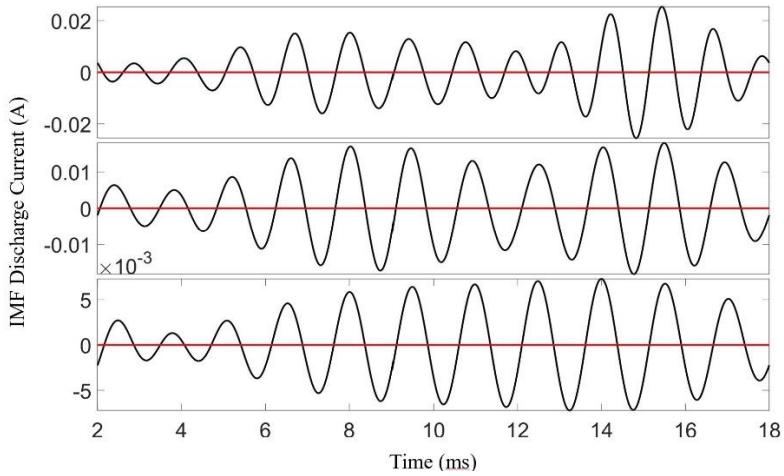

Figure 3 – Discharge Current IMFs

We apply the IMFogram algorithm in the nonlinear case for a more accurate representation of discharge voltage and current in the time-frequency domain when excessive harness inductance causes oscillations to be large relative to the DC operating point of the Hall thruster. The IMFogram technique is superior to the empirical mode decomposition (EMD) technique that is coupled to the Hilbert-Huang Transform for time-frequency analysis [15]. The EMD also uses IMFs as its basis, but it does not preserve Fourier energy and thus is not as accurate as the IMFogram. Other nonlinear transforms include the nonlinear FFT, the nonlinear STFT, and the empirical Fourier decomposition, though their present publicly available implementations depend on mathematically defined inputs rather than time series data [20, 21]. These techniques cannot be used to compute impedance, since no transfer function exists for nonlinear systems.

E. Reactive Power Analysis of a Hall Thruster Load

The reactive power as shown in figure 4 is either generated by capacitance in the load or is consumed by inductance in the load. This is a direct consequence of the impedance representations for each passive component. Using the frequency domain method presented in the previous section, it is possible to calculate the reactive power at each frequency in the load, since under the LTI assumption the frequencies can be treated separately. We further extend the power triangle by allowing for angles greater than 90 degrees, which allows for negative reactive powers that represent a production of reactive power. Knowing the reactive power allows one to compensate for it using known RLC impedance expressions and appropriately sizing RLC components, which can reduce oscillatory behavior in the discharge current and thus the discharge voltage.

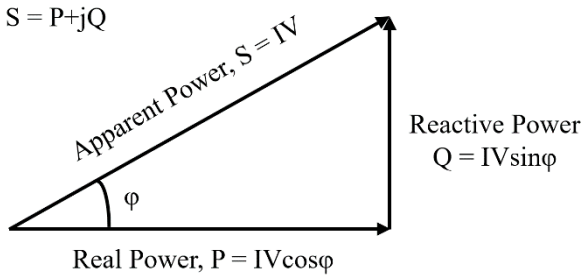

Figure 4 – Power Triangle Diagram

III. H9 Thruster Experimental/Simulink Simulations

Section A goes over the vacuum test facility that was used to conduct experimentation on the HET. Section B discusses the specific thruster used and its setup and operation. Section C explains the data collection process, section D describes noise analysis that justifies the use of the FFT at higher frequencies, section E discusses simulation details and data post-processing techniques, and lastly section F describes uncertainty quantification for the experiment.

A. Vacuum Facility

All experiments were performed in Vacuum Test Facility 2 (VTF-2) at the Georgia Institute of Technology High-Power Electric Propulsion Laboratory. A schematic of this facility is shown in Figure 5. VTF-2 is a stainless-steel chamber measuring 9.2 m in length and 4.9 m in diameter. VTF-2 is evacuated to a rough vacuum using one 495 CFM rotary-vane pump and one 3800 CFM blower. High vacuum is achieved using ten liquid nitrogen cooled CVI TMI re-entrant cryopumps. The cryopump shrouds are fed using the Stirling Cryogenics SPC-8 RL special closed-loop nitrogen liquefaction system [3].

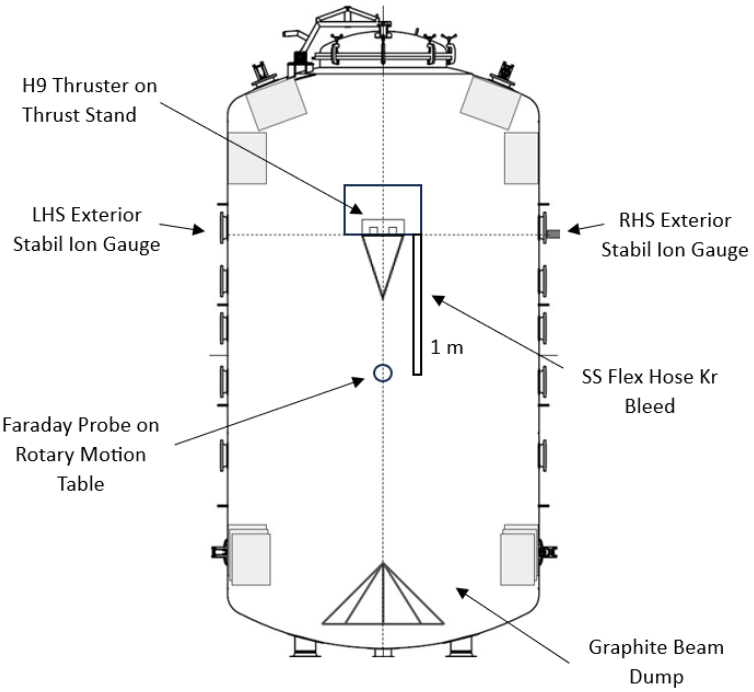

Figure 5 – VTF-2 Layout

B. H9 HET Setup and Operation

For this study, we used the H9 HET, shown in figure 6, a 9-kW class magnetically shielded Hall thruster developed in partnership between the University of Michigan, Jet Propulsion Laboratory, and the Air Force Research Laboratory (AFRL). The H9 employs a centrally mounted LaB_6 cathode. The performance of the H9 has been extensively mapped on krypton through prior investigations [22]. The thruster body was isolated from facility ground and cathode common and was electrically floating. Thruster body isolation was achieved via ceramic standoffs that isolate the thruster body from its support structures.

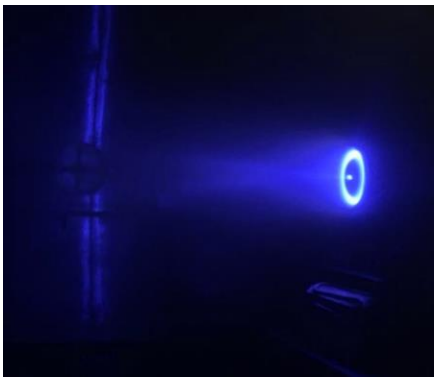

Figure 6 – Krypton-based Operation of H9 Hall Thruster

The H9 discharge was controlled using a Magna-Power TSA800-54 power supply. All other thruster components were powered using TDK-Lambda GEN80-42 power supplies. A TDK-Lambda GEN600-2.6 and GEN60-25 were used for the cathode keeper and heater, respectively. To protect the discharge supply from thruster oscillations, the discharge supply was connected to a low-pass discharge filter consisting of a series 0.533-Ω resistor and a shunt 100-μF capacitor to attenuate discharge current oscillations that are greater than 3 kHz in frequency.

High-purity (99.999%) krypton propellant was supplied to the anode and cathode lines using stainless-steel lines metered with MKS GE50A mass flow controllers (MFCs). The MFCs were calibrated by measuring the flow upstream of the thruster with a MesaLabs DryCal 800-10 volumetric flow meter. The uncertainty for the anode and cathode lines were 2% and 5%, respectively.

The power supply voltage, anode and cathode flow rate, and the magnetic field were kept constant during testing. The H9 thruster was operated for three hours until its oscillations became steady after outgassing. A discharge voltage of 300 V and a discharge current of 20 A were selected as the operating point of the thruster, which is small-signal linear, as determined by Jovel [12]. The facility pressure during operation was 6.236 μTorr.

C. Data Collection

The discharge current of the H9 Thruster was recorded using a Teledyne LeCroy CP150 current probe connected to a HDO6104 Teledyne LeCroy oscilloscope. The uncertainty and bandwidth of the current probe are ±1% and 10 MHz; for the oscilloscope, they are ±0.5% full scale and 1 GHz. The oscilloscope has 12 bits of resolution with a selected 25 MS/s sampling rate and is used over an interval of 20 ms for 500,000 samples in all. Thruster data was taken after it was observed that the peak-to-peak current values had stopped changing within ±1% variation, taking approximately two hours.

D. Noise Analysis

Time series analysis may be affected by measurement noise, especially if the noise floor exceeds the strength of a signal. Thus, noise measurements were conducted on each channel of each oscilloscope to characterize what was being read without any measurements of a signal of interest, so that it could be subtracted away when measuring the signal of interest. With the current probe not being clamped to any wire, the recorded noise signal was on average 40 mA. The total noise signal is distributed across a range of frequencies, with noise frequency components being roughly 0.1 mA in amplitude. Signal frequencies comparable and less in amplitude than the noise frequencies can be removed from time-frequency analysis. Furthermore, the remaining signal frequency components can be deemed significant when compared to the noise frequency components, thus validating the FFT approach.

E. Simulations and Post-Processing of Data

Simulink was used to generate discharge voltage using the same circuit used in the BMO model. Instead, the BMO load is replaced with experimental discharge current data. MATLAB was used to compute the frequency and time-frequency transforms.

F. Uncertainty Quantification

Systematic and random errors were quantified as part of this study's error analysis. Systematic errors are introduced by current probes, along with the oscilloscope, which were defined in the data collection subsection. Simulink and

MATLAB can also introduce errors. Random error includes noise contributions that may affect the FFT plot to a small extent.

IV. Results and Discussion

Section A explores a time-domain analysis of the breathing mode model, exploring the relationship between harness inductance and discharge oscillations. Section B looks at the time-domain of experimental discharge voltage and current waveforms. Section C investigates the impedance of experimental/simulation data at a harness inductance of 25.6 μH. Section D explores time-frequency analysis as applied to Hall thrusters. Lastly, section E presents an equivalent circuit model for a discharge plasma.

A. Time Domain Analysis (BMO)

Figure 7a and 7b show the discharge voltage and current oscillations produced by the BMO model at an inductance of 15 μH. The discharge voltage waveforms appear to be periodic but are not sinusoidal. The discharge current oscillations are almost sinusoidal and appear to be periodic as well. From inspection, the breathing mode frequency is approximately 20 kHz. However, when it is not known whether the thruster is operating at a linear operating point, it is best to use a nonlinear transform such as the IMFogram.

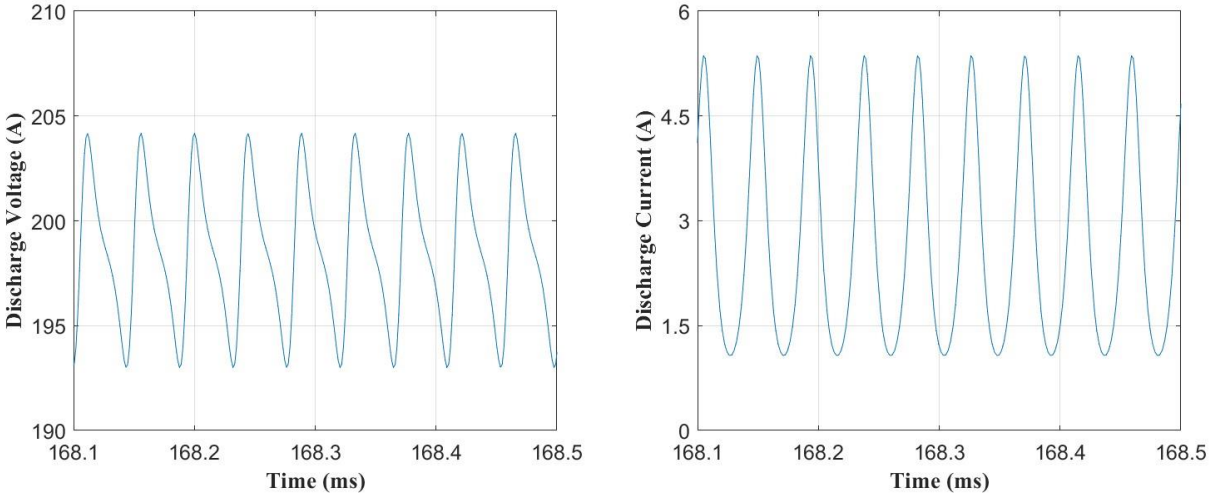

Figure 7 – Discharge Voltage (a) and Discharge Current (b) Oscillations at 15 μH

Figure 8a shows that the peak-to-peak values of the discharge voltage oscillation increases almost linearly with harness inductance, which matches results obtained by Pinero [10]. The discharge voltage peak-to-peak starts at 0 V at no harness inductance and increases to almost 40 V at 50 μH. The RMS in figure 8b also follows a similar characteristic, where the discharge voltage RMS increases from 198.5 V to 199.25 V from 0 to 50 μH, respectively. It is important to note that the di/dt of the discharge current waveforms of the BMO model do not match those of actual Hall thruster discharge current traces, leading to lower discharge voltage peak-to-peak values. The BMO model also suggests that inductance alone cannot be used to decrease discharge oscillations.

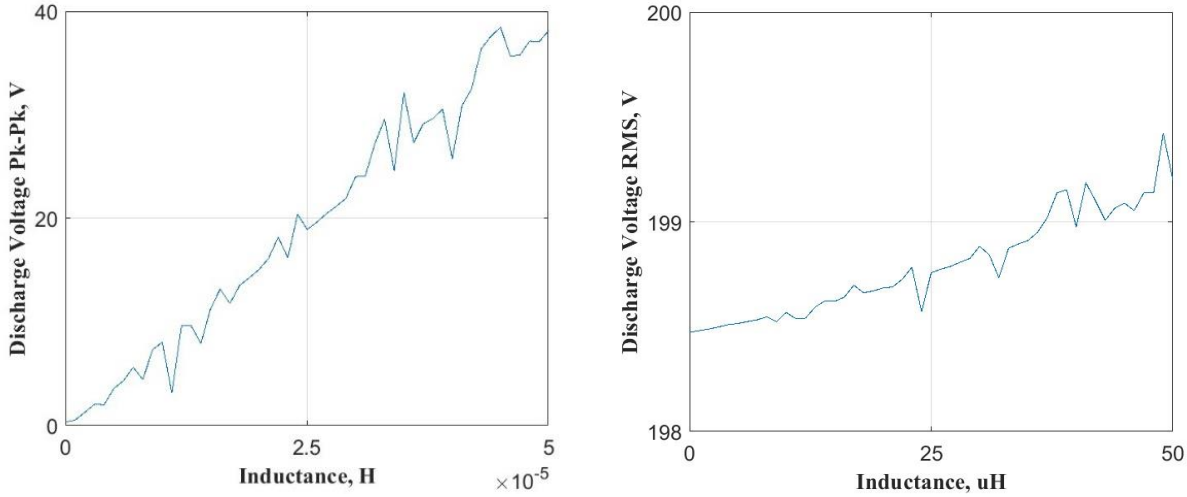

Figure 8 – Discharge Voltage Peak-to-Peak (a) and Discharge Voltage RMS (b) versus Harness Inductance

Both figure 9a and figure 9b show that discharge current oscillations do not change significantly over the harness inductance interval on average. This result makes sense, as a changing di/dt with increasing inductance would make the plots nonlinear, which is not the case. This contrasts with conventional loads where a high inductance decreases di/dt. This is likely not the case for a Hall thruster discharge plasma since there are many frequency components present in the discharge current, so compensation at one frequency results in further disturbing other frequency components.

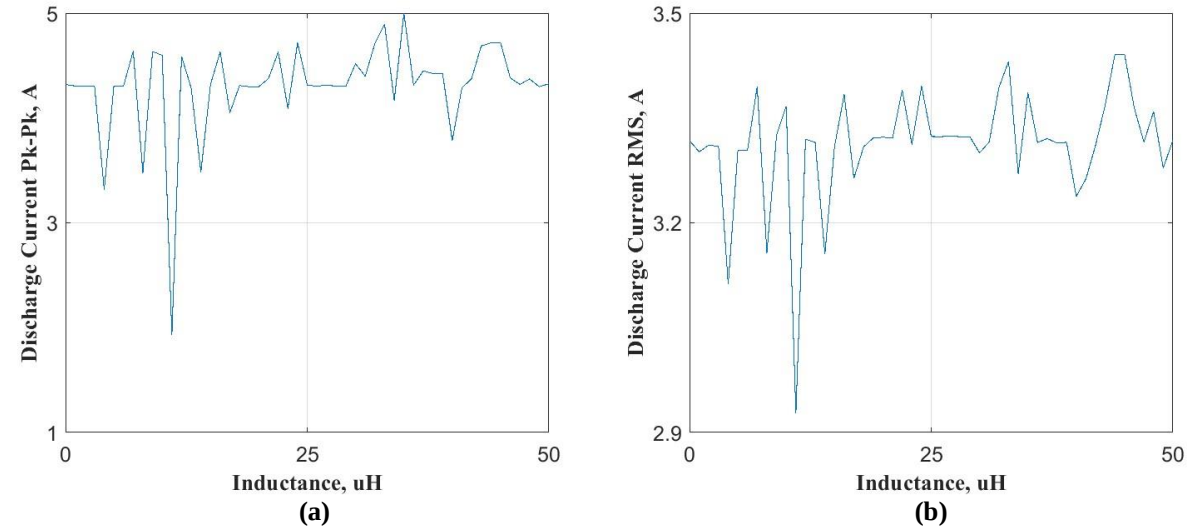

Figure 9 – Discharge Current Peak-to-Peak (a) and Discharge Current RMS (b) versus Harness Inductance

Figure 7a shows an impedance plot that has similar RLC characteristics as a transmission line impedance plot, where the impedance starts out as resistance, then becomes inductive, then encounters a resonance peak, and finally turns capacitive, though there are many more resonances after this regime. The RLC parameters up to 50 kHz are R = 2.387 Ω, L = 30.242 μH, and C = 201.26 nF. When the inductance is increased, the nature of the impedance plot changes, as seen in figure 7b, where the impedance starts out as resistive, then becomes capacitive and then inductive, leading to several more resonance peaks. The RLC parameters up to 10 kHz are R = 28.614 Ω, L = 110.47 μH, and C = 1.73 μF. These results further show how the inductance can play a significant role in changing the dynamics of a Hall thruster discharge plasma.

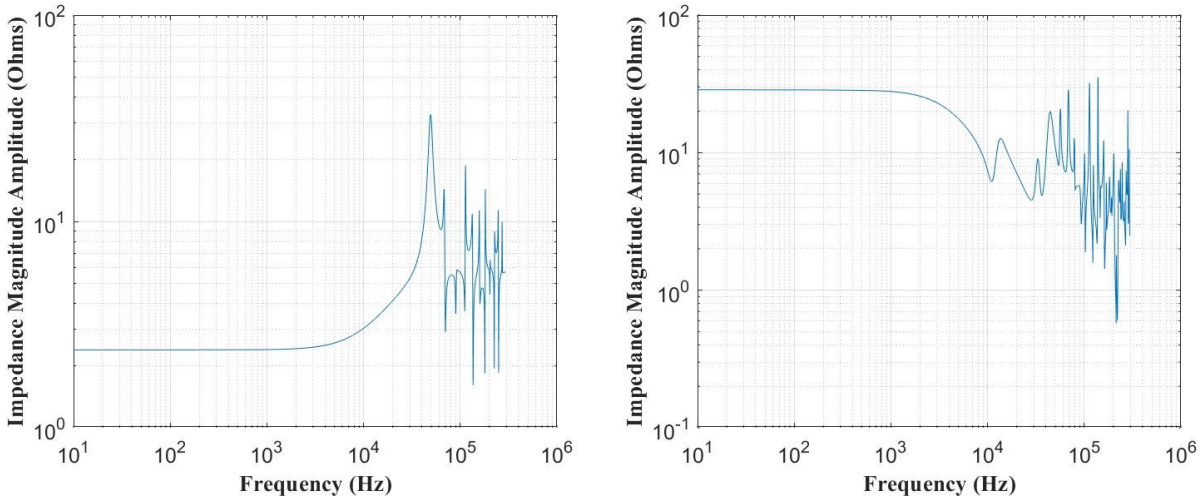

Figure 2 – Impedance-Frequency Magnitude Plots at Harness Inductances of 15 µH (a) and 20 µH (b)

Figure 10 shows the discharge oscillations at a harness inductance of 700 µH. Figure 10a shows that the discharge voltage attains negative values for a small portion of the oscillations. Figure 10b shows that the discharge current remains positive. Negative discharge voltages could affect the ionization process in a Hall thruster discharge plasma. The discharge voltage could go even lower when additional frequency components are considered beyond the BMO.

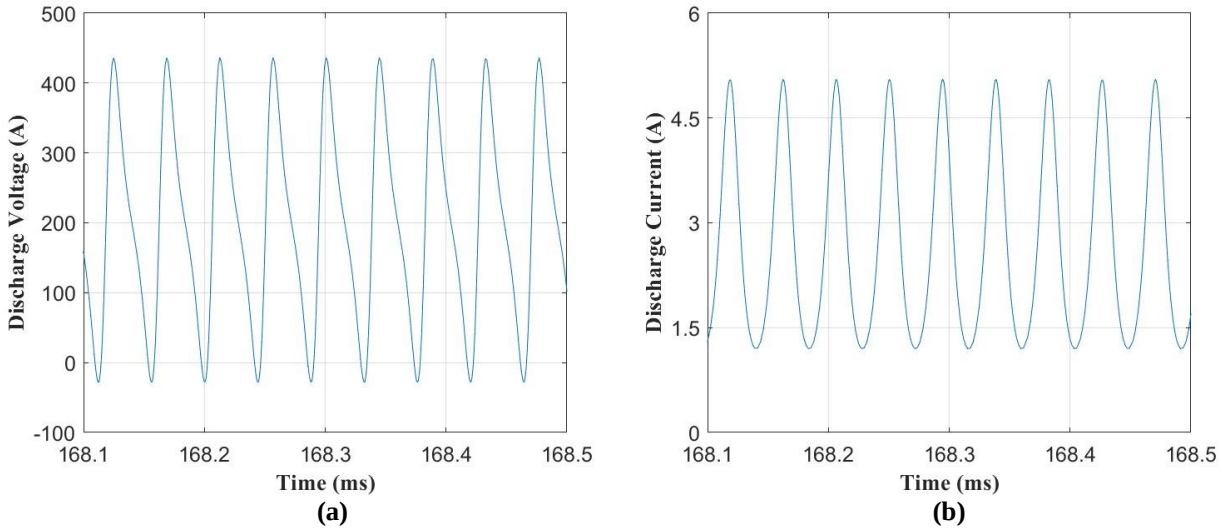

Figure 10 – Discharge Voltage (a) and Discharge Current (b) at Harness Inductance of 700 µH

B. Time Domain Analysis (Experimental/Simulation)

In the specific case where the harness inductance is 25.6 µH, the discharge voltage oscillation has a peak-to-peak of 284 V, shown in figure 11a. The discharge current oscillation has a peak-to-peak of 13.5 A as seen in figure 11b. Both waveforms exhibit considerably large amplitude oscillations taking around 30% of the mean for the discharge voltage, and around 50% of the mean for the discharge current.

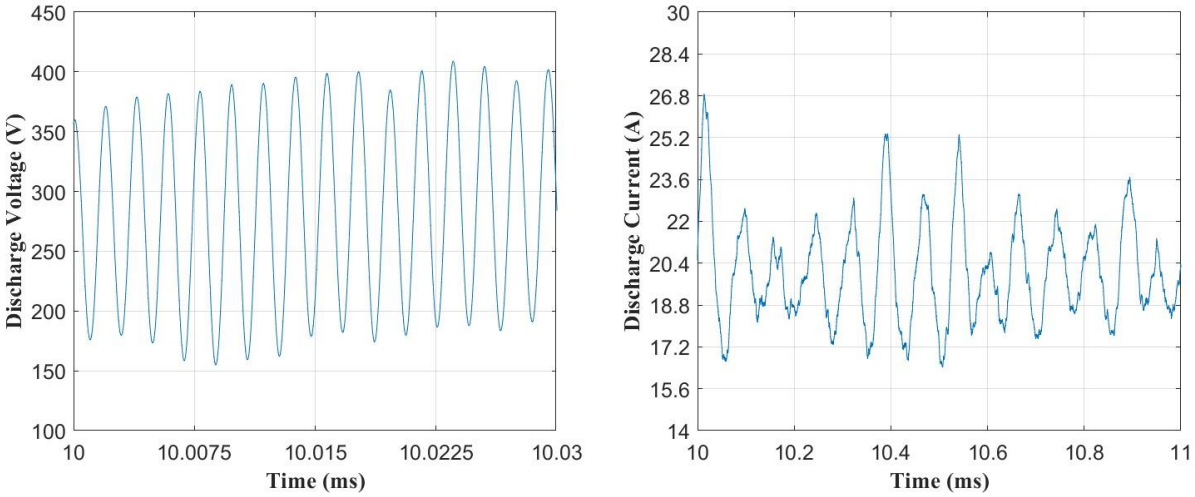

(a) (b)

Figure 11 – Simulated Discharge Voltage (a) and Experimental Discharge Current (b) Oscillations

C. Impedance Analysis (Experimental/Simulation)

The BMO frequency is 14.1 kHz, where both the discharge voltage and discharge current FFTs have a prominent peak, as seen in figures 12a and 12b. Of note is the second larger peak in the discharge voltage FFT at a frequency of around 510 kHz. This is likely due to circuit parasitics interacting with the discharge plasma, leading to a resonant peak.

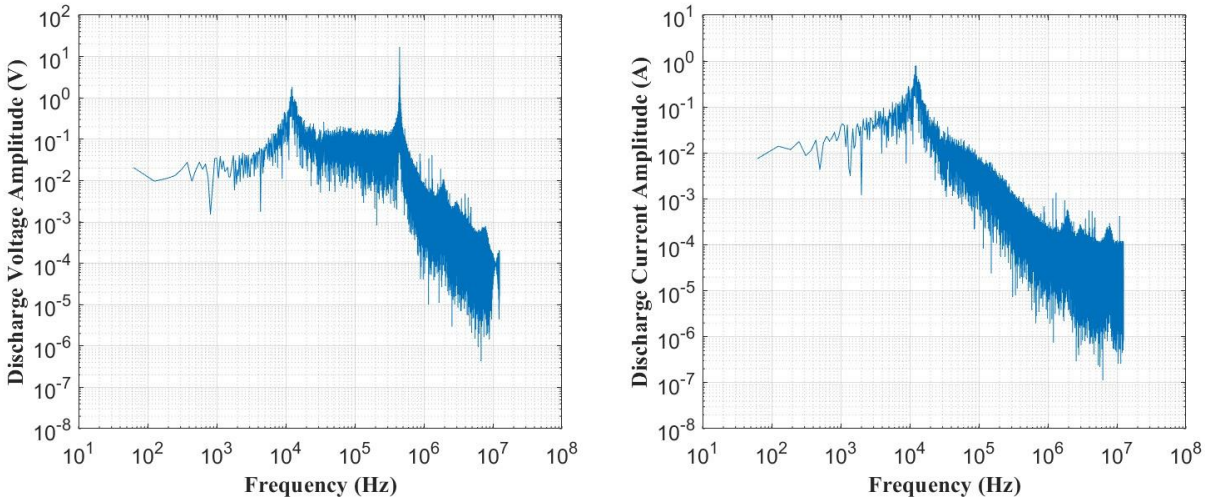

(a) (b)

Figure 12 – Simulated Discharge Voltage FFT (a) and Discharge Current FFT (b)

Figure 13a shows the impedance plot of the discharge plasma, where many resistive, inductive, and capacitive behaviors can be observed. These electrical properties are the result of motion of the various species in the discharge plasma. The averaged impedance plot of the discharge plasma in figure 13b appears to match the characteristic of a transmission line, where RDP = 1.85 Ω, LDP = 52.3 μH, and CDP = 1.74 nF. The BMO in figure 13c has a negative reactive power of −1.59 VAR, which indicates that the BMO has a capacitive component that produces reactive power. While the reactive power peaks at the breathing mode frequency, the impedance at the breathing mode frequency does not, illustrating that impedance and reactive power are different quantities.

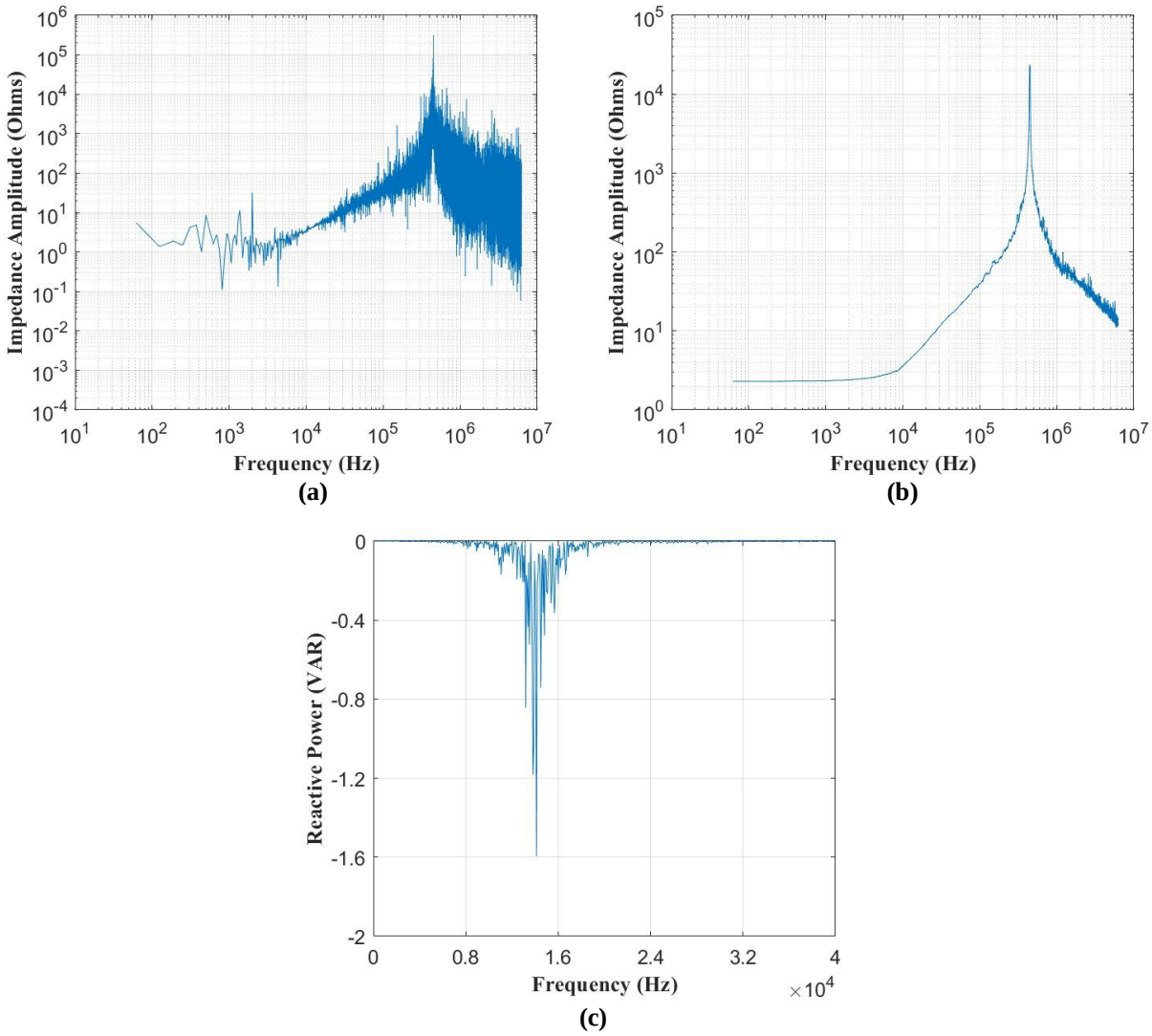

Figure 13 – Impedance-Frequency Magnitude Plot (a), Averaged Impedance-Frequency Magnitude Plot (b), and Reactive Power-Frequency Plot (c) of H9 Thruster

D. Time-Frequency Analysis (Experimental/Simulation)

Figure 14a shows resistance versus time, where the average value in the selected time window is 1.3 Ohms. Variation with time is significant, with a resistance peak-to-peak of 1 Ohm. Figure 14b shows inductance versus time, where the inductance on average is 50 uH. As with the resistance, the inductance changes significantly with time, with a peak-to-peak of 15 uH. The frequencies of the resistance, inductance, and capacitance correspond to the frequency range that they belong to in an impedance plot.

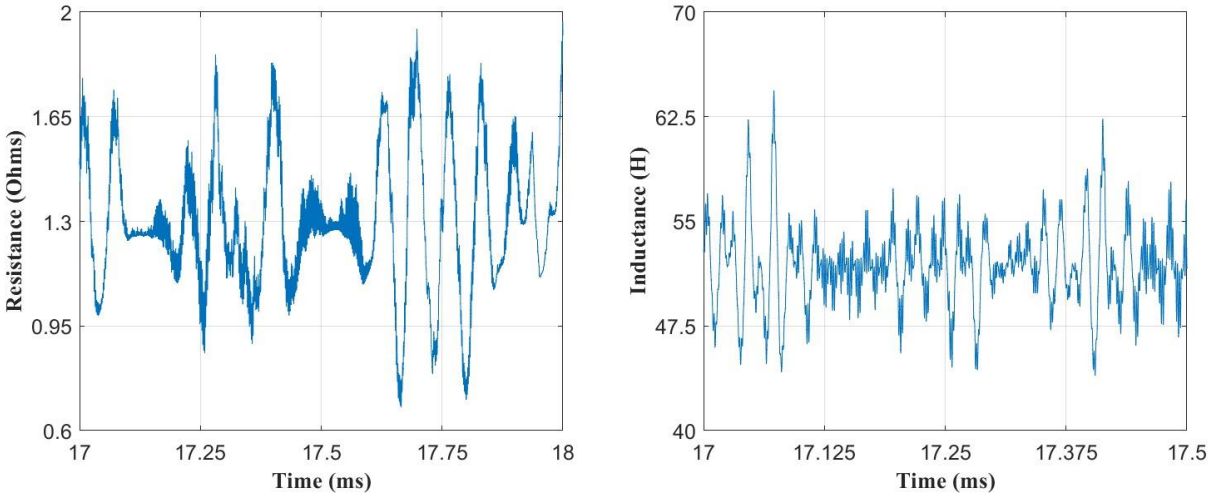

Figure 14 – Discharge Resistance (a) and Discharge Inductance (b) versus Time

Figure 15a shows that the capacitance changes by up to 2.5 nF in the selected time window, centered around 2.5 nF. Figure 15b shows the DC impedance versus time, where the impedance is approximately 14.3 Ohms. It is apparent that the DC impedance remains largely constant with time.

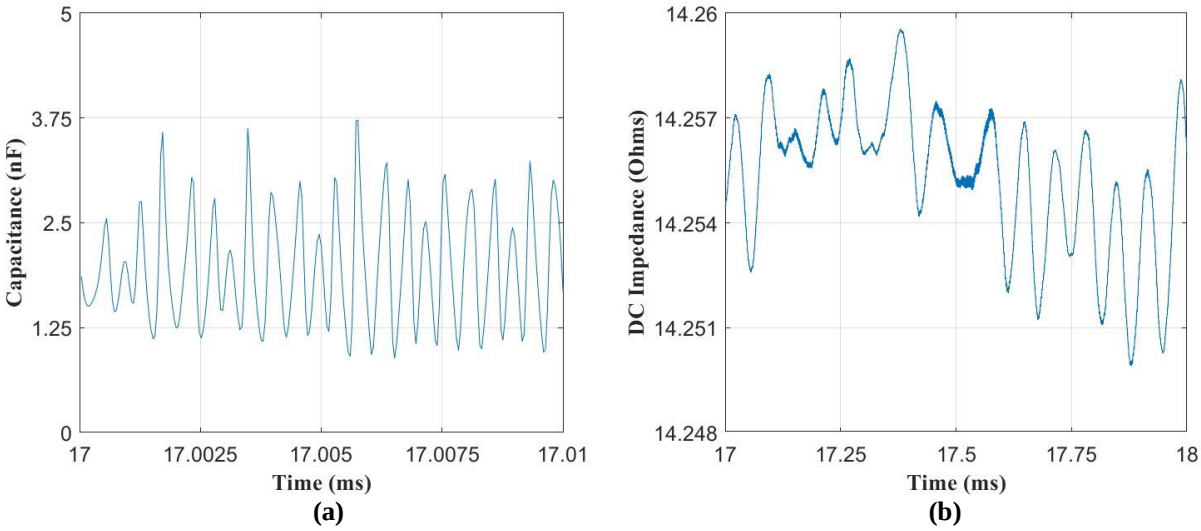

Figure 15 – Discharge Capacitance (a) and DC Impedance (b) versus Time

Figure 16a shows that changes in the BMO impedance with time are negligible. Changes in the impedance of the 500 kHz component change significantly, exhibiting a peak-to-peak of nearly 20,000 Ohms, as shown in figure 16b. The intense impedance fluctuations can be observed in the FFT impedance plots.

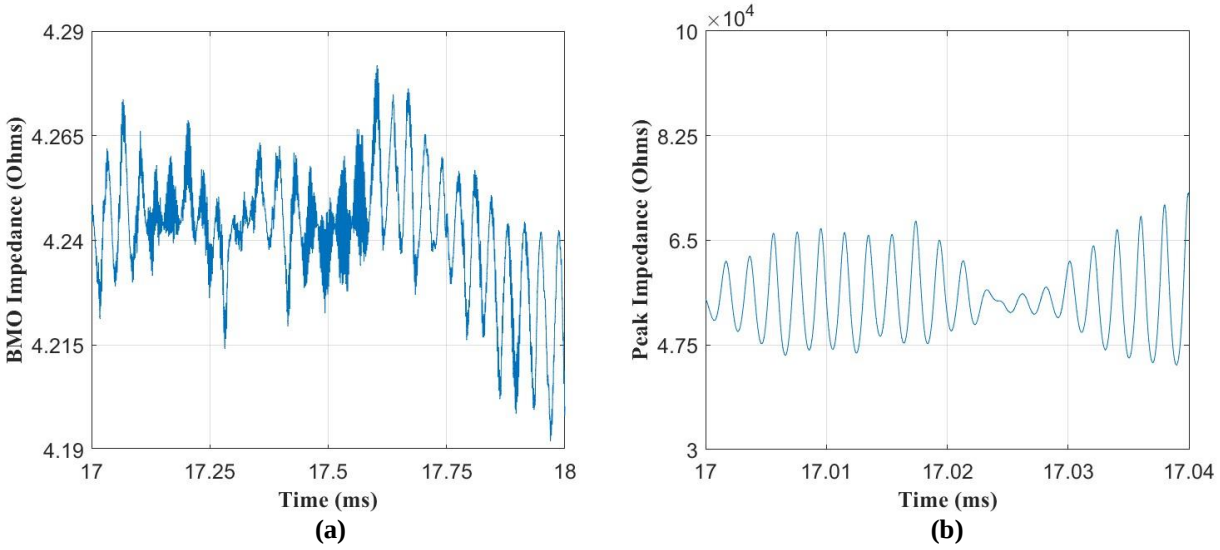

Figure 16 – BMO Impedance (a) and Peak Impedance (b) versus Time

Figure 17 shows the reactive power fluctuations of the BMO. The peak-to-peak value is 0.3 VAR. This value could be higher for higher power thrusters.

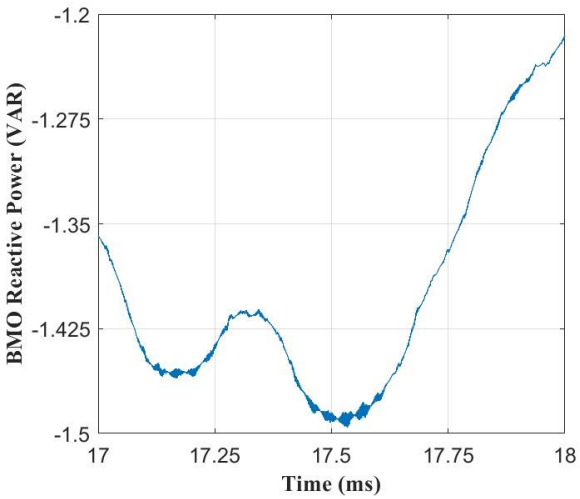

Figure 17 – BMO Reactive Power versus Time

Figures 18a and 18b show the discharge voltage and discharge current, respectively, in the time-frequency domain. It can be observed that there are several prominent lines in the plots, representing the peak impedance and BMO frequencies. The color map shows the intensity at a particular frequency and point in time. It is important to note how certain frequencies appear and disappear with time, showing how a Hall thruster discharge plasma is time-varying. The BMO frequency is 12.5 kHz when using the IMFogram, which is different than the 14.1 kHz obtained using the FFT. The peak impedance frequency 519 kHz, compared to 510 kHz using the FFT. This demonstrates the difference between using nonlinear nonstationary analysis versus linear time-invariant analysis. We must stop here in the impedance analysis as voltage and current IMFograms cannot be divided; a nonlinear transfer function does not exist.

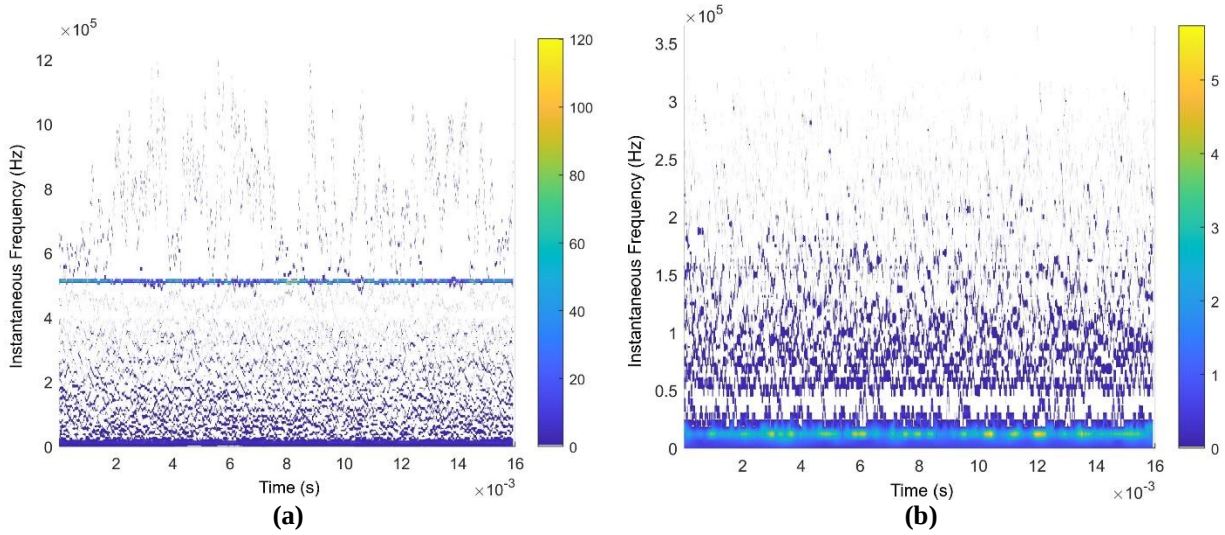

Figure 18 – Simulated Discharge Voltage IMFogram (a) and Experimental Discharge Current IMFogram (b)

E. Discharge Plasma Equivalent Circuit Model (Experimental/Simulation)

Figure 19 shows the equivalent discharge plasma load model integrated into the discharge circuit, given by RDP, LDP, and CDP. This model is only valid for AC components of the discharge. The equivalent AC circuit model is likely only valid for specific inductances.

A RLC compensation network can be designed to on average perform either impedance matching or reactive compensation. An example of such a network has been developed by Liqiu et al., which involves cascading two RLC filters [23-26]. Since reactive power is being produced, extra inductance may be needed to absorb the reactive power. The BMO model can be used as a starting point to simulate specific RLC networks to meet engineering design goals as a preliminary step.

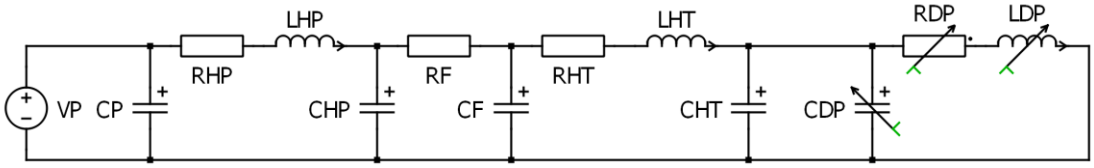

Figure 19 – Discharge Circuit with Equivalent AC Discharge Plasma Load Model at LHT = 25.6 µH

V. Conclusion

We show how inductance affects discharge voltage and current oscillations in a BMO model, particularly that increasing inductance increases oscillatory behavior. This can cause a Hall thruster to change from being considered linear time-varying to nonlinear time-varying. We also show how impedance can be computed from discharge voltage and current oscillations using FFT and STFT approaches applied to the BMO model and experimental/simulation data, an improvement over a previous approach. Inductance plays a significant role in the impedance characteristics of the Hall thruster discharge plasma. We also demonstrate the IMFogram approach, which is the most general approach that makes the least assumptions about the Hall thruster system, which is nonlinear and time varying. It represents an accurate way to represent discharge oscillations in the time-frequency domain, however impedance cannot be calculated in any nonlinear case, whether time invariant or time varying.

The conventional wisdom is to place the filter as close as possible to the thruster, which is not always feasible. Instead, it is possible to place additional RLC networks between the discharge filter and the thruster to reduce current and thus voltage oscillations to address harness facility effects. Rather than just focusing on harness inductance alone, we focus on the total impedance in the discharge circuit including the load.

Analyzing the impedance of the Hall thruster discharge plasma allows one to better understand Hall thruster dynamics, as the impedance at each frequency is related to the reactive power at each frequency. The reactive power represents how oscillatory a load is and compensating for it using RLC networks is one way to reduce oscillations.

However, one must be careful not to place too much inductance between the filter and the thruster, as this could lead to negative discharge voltages, which may adversely affect Hall thruster performance. The ability to calculate additional parameters such as R, L, C, impedance, and reactive power allow for additional ways to diagnose a Hall thruster discharge plasma as a function of time.

Acknowledgments

The authors would like to thank Dr. Haomin Zhou of the School of Mathematics at the Georgia Institute of Technology for providing guidance on how to use the IMFogram approach to analyze a nonlinear time varying system in the frequency domain, as well as Dr. Andrew Peterson of the School of Electrical and Computer Engineering for providing additional guidance on transmission line effects. Additionally, we would like to thank Emma Li, Frank George, Jake Wiersma, and Chris McCollough, who are undergraduates at the Georgia Institute of Technology that assisted with the experimental setup and vacuum facility operation. Lastly, the authors would like to thank the NASA Joint Advanced Propulsion Institute for its support under the grant number 80NSSC21K1118.

References

[1] D. M. Goebel, I. Katz, I. G. Mikellides *Fundamentals of Electric Propulsion* (Wiley, 2023).

[2] Byers, D. and Dankanich, J. W., "A review of facility effects on Hall effect thrusters," *31st International Electric Propulsion Conference*, Sep. 2009.

[3] Dankanich, J. W., Walker, M. L. R., Swiatek, M. W., and Yim, J. T., "Recommended practice for pressure measurement and calculation of effective pumping speed in electric propulsion testing," *Journal of Propulsion and Power*, vol. 33, May 2017, pp. 668–680.

[4] Frieman, J. D., King, S. T., Walker, M. L. R., Khayms, V., and King, D., "Role of a conducting vacuum chamber in the Hall Effect Thruster Electrical Circuit," *Journal of Propulsion and Power*, vol. 30, Nov. 2014, pp. 1471–1479.

[5] Walker, J. A., Langendorf, S. J., Walker, M. L. R., Khayms, V., King, D., and Peterson, P., "Electrical facility effects on hall current thrusters: Electron termination pathway manipulation," *Journal of Propulsion and Power*, vol. 32, Nov. 2016, pp. 1365–1377.

[6] Byrne, M. P., Roberts, P. J., and Jorns, B. A., "Coupling of electrical and pressure facility effects in Hall effect thruster testing," *37th International Electric Propulsion Conference*, Jun. 2022.

[7] Choueiri, E. Y., "Plasma oscillations in hall thrusters," *Physics of Plasmas*, vol. 8, Apr. 2001, pp. 1411–1426.

[8] Fife, J., Martinez-Sanchez, M., and Szabo, J., "A numerical study of low-frequency discharge oscillations in hall thrusters," *33rd Joint Propulsion Conference and Exhibit*, Jul. 1997.

[9] Leporini, L., Giannetti, V., Saravia, M. M., Califano, F., Camarri, S., and Andreussi, T., "On the onset of breathing mode in hall thrusters and the role of electron mobility fluctuations," *Frontiers in Physics*, vol. 10, Aug. 2022.

[10] Pinero, L. R., "The Impact of Harness Impedance on Hall Thruster Discharge Oscillations," *35th International Electric Propulsion Conference*, Oct. 2017.

[11] Brieda, L., Koo, J., and Scharfe, M., "Influence of a power supply model on simulated Hall thruster discharge voltage oscillations," *AIP Advances*, 2019.

[12] Jovel, D. R., "Impedance Characterization of a Hall Effect Thruster Discharge in a Ground-Based Vacuum Test Facility," *PhD Thesis*, 2024.

[13] Lyu, C. L., Liu, H., Luo, W., Zhang, T., and Zhao, W., "A Fast Time Domain Measuring Technique of Electrochemical Impedance Spectroscopy Based on FFT," *Prognostics and System Health Management Conference*, 2018.

[14] Kurzyna, S., Mazouffre, S., Lazurenko, A., Albarede, L., Bonhomme, G., Makowski, K., Dudeck, M., and Peradzynski, Z., "Spectral analysis of Hall-effect thruster plasma oscillations based on the empirical mode decomposition," *Physics of Plasmas*, 2005.

[15] Cicone, A., Li, W. S., and Zhou, H., "New theoretical insights in the decomposition and time-frequency representation of nonstationary signals: the IMFogram algorithm," *arXiv*, 2022.

[16] Troyetsky, D. E., Greve, C. M., Tsikata, S., and Hara, K., "State estimation for real-time analysis of dynamic plasma properties and electrical circuit effects in Hall effect thrusters," *37th International Electric Propulsion Conference*, Jun. 2022.

[17] Hoshi, Y., Yakabe, N., Isobe, K., Saito, T., Shitanda, I., and Itagaki, M., "Wavelet transformation to determine impedance spectra of lithium-ion rechargeable battery," *Journal of Power Sources*, 2016.

[18] Gomez-Luna, E., Silva, D., Aponte, G., Pleite, J. G., and Hinestroza, D., "Obtaining the Electrical Impedance Using Wavelet Transform From the Time Response," *IEEE Transactions on Power Delivery*, 2013.

[19] Xu, S., Zhang, Z., Zhang, Z., Yang, W., Tang, H., and Ling, W., "Time-frequency-domain method for thrust noise characteristics of electric thrusters," *Acta Astronautica*, 2022.

[20] Tao, T. and Thiele, C., "Nonlinear Fourier Analysis," *arXiv*, 2012.

[21] Singh, P., Joshi, S. D., Patney, R. K., and Saha, K., "The Fourier decomposition method for nonlinear and non-stationary time series analysis," *Proceedings of the Royal Society A*, 2017.

[22] Su, L. L., Vazsonyi, A. R., and Jorns, B., "Performance of a 9-kW Magnetically-Shielded Hall thruster with Krypton," *AIAA Propulsion and Energy 2020 Forum*, Aug. 2020.

[23] Barral, S. and Miedzik, J., "Numerical investigation of closed-loop control for Hall accelerators," *Journal of Applied Physics*, 2011.

[24] Liqiu, W., Chunsheng, W., Zhongxi, N., Weiwei, L., ChaoHai, Z., and Daren, Y., "Experimental study on the role of a resistor in the filter of Hall thrusters," *Physics of Plasmas*, 2011.

[25] Liqiu, W., Zhongxi, N., Peng, E., and Daren, Y., "On the frequency characteristic of inductor in the filter of Hall thrusters," *Journal of Vacuum Science and Technology*, 2010.

[26] Liqiu, W., Jing, L., Liang, H., Daren, Y., Chaohai, Z., and Xiaobin, H., "Stabilizing Low Frequency Oscillation with Two Stages Filter in Hall thrusters," *30th International Electric Propulsion Conference*, July 2015.